JACS
JOURNAL OF THE AMERICAN CHEMICAL SOCIETY
Article
pubs.acs.org/JACS

Topochemical Nitridation with Anion Vacancy-Assisted N^{3-}/O^{2-} Exchange

Riho Mikita,[†] Tomoko Aharen,[†] Takafumi Yamamoto,[†] Fumitaka Takeiri,[†] Tang Ya,[†] Wataru Yoshimune,[†] Koji Fujita,[‡] Suguru Yoshida,[‡] Katsuhisa Tanaka,[‡] Dmitry Batuk,[§] Artem M. Abakumov,[§,∥] Craig M. Brown,[⊥] Yoji Kobayashi,[†,#] and Hiroshi Kageyama*[,†,▽]

[†]Department of Energy and Hydrocarbon Chemistry, Graduate School of Engineering and [‡]Department of Material Chemistry, Graduate School of Engineering, Kyoto University, Nishikyo-ku, Kyoto 615-8510, Japan
[§]Electron Microscopy for Materials Research (EMAT), University of Antwerp, Groenenborgerlaan 171, B-2020 Antwerp, Belgium
[∥]Skoltech Center for Electrochemical Energy Storage, Skolkovo Institute of Science and Technology, 143026 Moscow, Russia
[⊥]Center for Neutron Research, National Institute of Standards and Technology, Gaithersburg, MD 20899, United States
[#]PRESTO and [▽]CREST, Japan Science and Technology Agency (JST), Kawaguchi, Saitama 332-0012, Japan

Supporting Information

ABSTRACT: We present how the introduction of anion vacancies in oxyhydrides enables a route to access new oxynitrides, by conducting ammonolysis of perovskite oxyhydride $EuTiO_{3-x}H_x$ ($x \sim 0.18$). At 400 °C, similar to our studies on $BaTiO_{3-x}H_x$, hydride lability enables a low temperature direct ammonolysis of $EuTi^{3.82+}O_{2.82}H_{0.18}$, leading to the N^{3-}/H^--exchanged product $EuTi^{4+}O_{2.82}N_{0.12}\square_{0.06}$. When the ammonolysis temperature was increased up to 800 °C, we observed a further nitridation involving N^{3-}/O^{2-} exchange, yielding a fully oxidized $Eu^{3+}Ti^{4+}O_2N$ with the $GdFeO_3$-type distortion (*Pnma*) as a metastable phase, instead of pyrochlore structure. Interestingly, the same reactions using the oxide $EuTiO_3$ proceeded through a 1:1 exchange of N^{3-} with O^{2-} only above 600 °C and resulted in incomplete nitridation to $EuTiO_{2.25}N_{0.75}$, indicating that anion vacancies created during the initial nitridation process of $EuTiO_{2.82}H_{0.18}$ play a crucial role in promoting anion (N^{3-}/O^{2-}) exchange at high temperatures. Hence, by using (hydride-induced) anion-deficient precursors, we should be able to expand the accessible anion composition of perovskite oxynitrides.

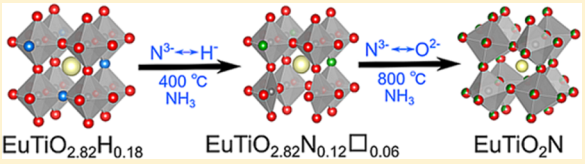

INTRODUCTION

Perovskite oxynitrides, ABO_2N and $ABON_2$, have received considerable attention owing to their novel properties that are unattainable in simple oxides, including visible-light photocatalysis in $LaTiO_2N$,[1,2] dielectric properties in $ATaO_2N$ (A = Ba, Sr),[3,4] and colossal magnetoresistivity in $EuNbO_2N$ and $EuWON_2$.[5,6] Most of these oxynitrides have been prepared through annealing under flowing ammonia gas (ammonolysis). In general, nontopochemical ammonolysis reactions require high temperatures (800−1500 °C) to allow diffusion of constituent cations of starting reagents (e.g., oxides and carbonates),[7] as in the case of oxides. For example, $BaTaO_2N$ is synthesized by ammonolysis of a stoichiometric mixture of $BaCO_3$ and Ta_2O_5 at 950−1000 °C.[3] However, the severity of high temperature ammonolysis considerably limits the compositional variation of oxynitrides. For example, the B site is mostly occupied by early transition metals (e.g., Ti^{4+}, Nb^{5+}, Ta^{5+}, $W^{6+/5+}$) that are robust against the highly reducing atmosphere.[7] Due to this highly reducing environment, europium in perovskite oxynitrides is known to adopt a divalent state ($EuTaO_2N$ and $EuNbO_2N$),[5] except for $EuWO_{1+x}N_{2-x}$ ($-0.16 \le x \le 0.46$, $Eu^{(2-2.16)+}$),[6] putting a significant constraint on chemical and physical properties.

Another notable feature in perovskite oxynitrides is the fact that the total anion content is (almost) 3. For example, the cation choices of (A, B) = (Sr, Nb), (La, Nb), and (La, Ti) simply give $SrNbO_2N$, $LaNbON_2$, and $LaTiO_2N$, respectively, apart from a small deviation from stoichiometry for the anion.[8] This is in stark contrast to most oxide perovskites (ABO_3), whose anion content can be widely varied (depending on the A and B cations), often yielding anion vacancy-ordered structures such as the brownmillerite structure $ABO_{2.5}$ or the infinite layer structure ABO_2.[9] It is not clear why oxynitrides with a significant amount of anion vacancies are absent, but this fact, together with a theoretically suggested lower N^{3-} diffusion (vs O^{2-}),[10] may introduce a kinetic issue during ammonolysis even at high temperatures. Also, the fact that most of the B-cations constituting oxynitrides (such as Ti^{4+}, Nb^{5+}, and Ta^{5+}) demonstrate strong affinity toward octahedral anion coordination may play a certain role in the negligibly small anion deficiency.

We have recently demonstrated a new topochemical route to access an oxynitride at rather low temperatures using an oxyhydride instead of a pristine oxide.[11,12] Here, the lability of

Received: January 5, 2016
Published: February 8, 2016

DOI: 10.1021/jacs.6b00088
J. Am. Chem. Soc. 2016, 138, 3211−3217

H^- anion in $BaTi^{(4-x)+}O_{3-x}H_x$ ($x \leq 0.6$) enables N^{3-}/H^- exchange at 375−550 °C, yielding the ferroelectric oxynitride $BaTi^{4+}O_{3-x}N_{2x/3}\square_{x/3}$. In this study, we have applied this strategy to $EuTiO_{3-x}H_x$, prepared by a CaH_2 reduction of $EuTiO_3$.[13] As shown in the lower portion of Scheme 1,

Scheme 1. Ammonolysis of $EuTiO_{2.82}H_{0.18}$ and $EuTiO_3$[a]

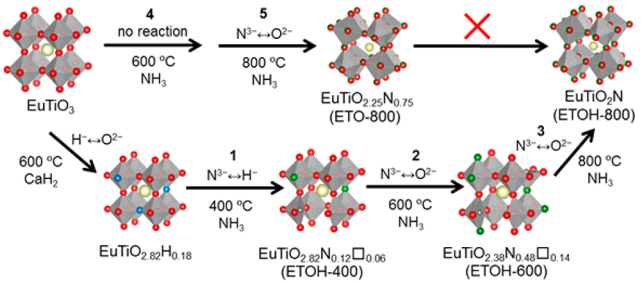

[a]The cubic oxyhydride $EuTiO_{2.82}H_{0.18}$ changes to $EuTiO_{2.82}N_{0.12}\square_{0.06}$ by ammonolysis at 400 °C, followed by conversion to $EuTiO_{2.38}N_{0.48}\square_{0.14}$ with an increased anion vacancy at 600 °C, and finally to fully oxidized $EuTiO_2N$ with the $GdFeO_3$-type structure at 800 °C. On the other hand, the ammonolysis of $EuTiO_3$ at 600 and 800 °C, respectively, resulted in no reaction and lower N content, $EuTiO_{2.25}N_{0.75}$. Yellow, gray, red, blue, and green spheres represent Eu, Ti, O, H, and N.

ammonolysis at 400 °C successfully converts $EuTiO_{2.82}H_{0.18}$ to $Eu^{2+}Ti^{4+}O_{2.82}N_{0.12}\square_{0.06}$. However, unexpectedly, when the ammonolysis temperature is increased up to 800 °C, further oxidative nitridation involving *an N^{3-}/O^{2-} exchange* proceeds and yields $Eu^{3+}Ti^{4+}O_2N$ as a thermodynamically metastable phase. We investigate compositions and crystal structures of $EuTiO_{2.82}H_{0.18}$ as well as $EuTiO_3$-ammonolyzed phases at various temperatures (400−800 °C) and discuss how the unprecedented high temperature topochemical reactions proceed, in particular, shedding light on the role of anion vacancies in directing the reaction toward the terminal metastable phase.

EXPERIMENTAL SECTION

$EuTiO_{3-x}H_x$, $EuTiO_3$, and $Eu_2Ti_2O_7$ were used as precursors for nitridation. $Eu_2Ti_2O_7$ and $EuTiO_3$ with pyrochlore and perovskite structures, respectively, were prepared by the polymerized complex method using $Ti(O^iPr)_4$ (97%, Sigma-Aldrich) and $Eu(NO_3)_3{\cdot}nH_2O$ (99.9%, Rare Metallic Co. Ltd.) as described in the literature.[13] $EuTiO_{3-x}H_x$ ($x \sim 0.18$) was prepared by reducing $Eu_2Ti_2O_7$ with a 2.5 molar excess of CaH_2 (99.99%, Sigma-Aldrich) in a sealed, evacuated Pyrex tube at 600 °C for 2 days. The residual CaH_2 and the byproduct CaO were removed by washing with a 0.1 mol/L NH_4Cl solution in methanol under vigorous and continuous stirring for 3 h.

The obtained powder ($EuTiO_{2.82}H_{0.18}$, $EuTiO_3$, $Eu_2Ti_2O_7$) was placed in a platinum boat in a tubular furnace for ammonolysis reactions. The tube was initially purged with dry N_2 gas and then with dry NH_3 gas at ambient temperature to expel oxygen and moisture before heating. Under ammonia gas flowing at 300 mL/min, the sample was heated to various temperatures T_R (400 °C $\leq T_R \leq$ 1000 °C) at 4.5 °C/min, held for 12 h, and cooled to 30 °C at 7 °C/min. $EuTiO_{2.82}H_{0.18}$ and $EuTiO_3$ after ammonolysis at T_R will be hereafter abbreviated, respectively, as ETOH-T_R and ETO-T_R (e.g., ETOH-800 and ETO-800 when T_R = 800 °C).

We characterized the purity and crystal structures of the samples by powder X-ray diffraction (XRD) measurements using a D8 ADVANCE diffractometer (Bruker AXS) with Cu-K_α radiation. High resolution synchrotron powder XRD experiments (SXRD) were also performed at room temperature using a Debye−Scherrer camera with an imaging plate as a detector, installed at SPring-8 BL02B2 of the Japan Synchrotron Radiation Research Institute (JASRI). Incident beams from a bending magnet were monochromatized to λ = 0.420671 Å, 0.420887 Å or 0.419795 Å. Sieved powder samples (<32 μm) were loaded into Pyrex capillaries with an i.d. of 0.2 mm. The sealed capillary was rotated during measurements to reduce the effect of preferred orientation. The collected SXRD patterns were analyzed by the Rietveld method using the RIETAN-FP program.[14]

To estimate the oxygen content of $EuTiO_{3-x}H_x$, we conducted a thermogravimetry (TG) measurement with a Bruker AXS TG-DTA 2000S under flowing O_2 at 300 mL/min up to 700 °C. A platinum pan was used as a sample holder and Al_2O_3 as a reference. Hydrogen release upon heating was monitored under flowing Ar at 300 mL/min by a Bruker MS9610 quadrupole mass spectrometer connected to the TG instrument.

To determine the anion composition of ETOH-800, neutron diffraction (ND) data were collected at room temperature using the high resolution powder diffractometer BT-1 at the NIST Center for Neutron Research (NCNR) and processed by Rietveld refinement. To reduce absorption effects from Eu, the sample was thinly spread on aluminum foil, wrapped to form an annulus, and placed inside a vanadium cylinder (diameter 12.4 mm, height 50 mm). We employed a vertical-focused Cu(311) monochromator and a premonochromator collimation of 60″, resulting in the maximum obtainable flux and a wavelength of 1.54060 Å.

Electron diffraction (ED) patterns of ETOH-800 were recorded using a FEI Tecnai G2 transmission electron microscope operated at 200 kV. The specimen for ED was prepared by grinding the powder sample under ethanol and depositing a drop of the suspension onto a copper grid covered with a holey carbon film. The sample consists of nanoparticles about 50−200 nm in diameter. Most of them form aggregates up to a micron. Zone axis ED patterns were acquired on individual particles.

The presence/absence of nitrogen in the samples was examined by the combustion method (elemental analysis) at Analytical Services, School of Pharmacy, Kyoto University. Approximately 2 mg of a sample was used each time, and three data sets were averaged. Magnetic susceptibilities were measured on a Quantum Design MPMS-XL SQUID magnetometer, with an applied magnetic field of 0.05 T from 2 to 300 K. ^{151}Eu Mössbauer spectra of ETOH-800 and ETO-800 were collected at room temperature in transmission geometry using a $^{151}Sm_2O_3$ γ-ray source. The source velocity was calibrated by EuF_3 as a standard.

RESULTS AND DISCUSSION

XRD patterns of $EuTiO_{3-x}H_x$ and $EuTiO_3$ were characterized by the cubic perovskite structure ($Pm\bar{3}m$) with a = 3.9143(1) Å and a = 3.90402(4) Å, respectively, while those of $Eu_2Ti_2O_7$ were indexed by the pyrochlore structure ($Fd\bar{3}m$) with a = 10.2071(1) Å (Figure S1), all in agreement with previous studies.[13,15,16] All of the precursors were single phases. Rietveld refinement of SXRD data of $EuTiO_{3-x}H_x$ (Figure S2 and Table S1) gave an oxygen content of 2.85(2), in reasonable agreement with 2.82 obtained from TG (Figure S3). As a result of electron doping, $EuTi^{3.82+}O_{2.82}H_{0.18}$ undergoes a ferromagnetic transition at T_C = 12 K (Figure 1a and Figure S4) due to the Ruderman−Kittel−Kasuya−Yosida (RKKY) interaction, as shown previously.[13]

Our recent study on $BaTi^{(4-x)+}O_{3-x}H_x$ ($x \leq 0.6$)[11] has demonstrated that hydride lability enables N^{3-}/H^- exchange with low temperature ammonolysis at 375−550 °C, yielding the fully oxidized $BaTi^{4+}O_{3-x}N_{2x/3}\square_{x/3}$. Hence, one can expect that such a low temperature ammonolysis for $Eu^{2+}Ti^{(4-x)+}O_{3-x}H_x$ will yield $Eu^{2+}Ti^{4+}O_{3-x}N_{2x/3}\square_{x/3}$. This is indeed what has happened for $EuTiO_{2.82}H_{0.18}$ (**1** in Scheme 1); the Rietveld refinement of the SXRD data for ETOH-400 converged adequately, yielding the composition $EuTiO_{2.90(2)}$

DOI: 10.1021/jacs.6b00088
J. Am. Chem. Soc. 2016, 138, 3211−3217

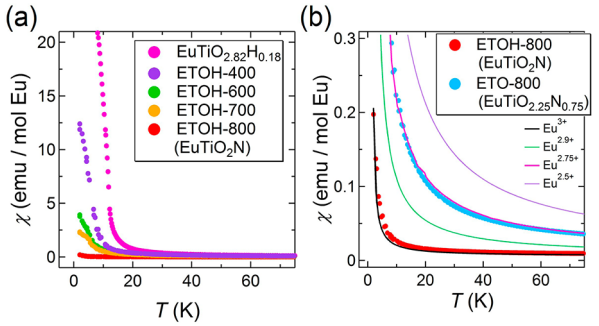

Figure 1. (a) Temperature dependence of the magnetic susceptibilities of $EuTiO_{2.82}H_{0.18}$ and the nitridized samples prepared at T_R = 400, 600, 700, and 800 °C, measured at 0.05 T. (b) An enlarged plot for ETOH-800 ($EuTiO_2N$). Solid lines are theoretical curves for Eu^{3+}, $Eu^{2.9+}$, $Eu^{2.75+}$, and $Eu^{2.5+}$ based on Van Vleck theory (details described in Supporting Information). ETO-800 ($EuTiO_{2.25}N_{0.75}$) is also plotted.

(i.e., $EuTi(O,N)_{2.90(2)}$). Here, an oxygen-deficient $EuTiO_{3-\delta}$ was assumed because of the negligible difference in X-ray scattering power of O and N. All the SXRD peaks of ETOH-400 ($EuTiO_{2.82}H_{0.18}$ after ammonolysis at T_R = 400 °C) were readily indexed by a cubic unit cell (a = 3.9103(1) Å), and its structure was refined using the ideal perovskite structure (Figure 2a and Table 1). ETOH-400 exhibits an antiferromagnetic transition at ~5 K (Figure 1a and Figure S4) as observed in $EuTiO_3$ and discussed in ref 13, indicating a complete loss of 3d electrons[17] (and thus a loss of hydrogen) by the oxidative nitridation. Furthermore, elemental analysis gave a nitrogen content of 0.67 wt %. From these results, we concluded that the chemical composition of ETOH-400 is $Eu^{2+}Ti^{4+}O_{2.82}N_{0.12}\square_{0.06}$.

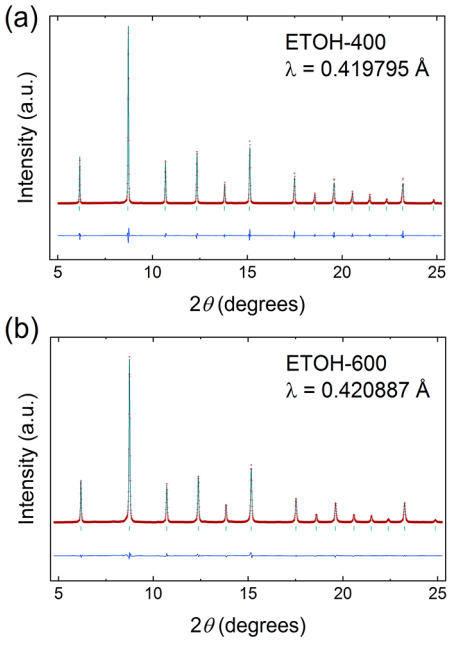

Figure 2. Observed and refined SXRD patterns for (a) ETOH-400 ($EuTiO_{2.82}N_{0.12}\square_{0.06}$) and (b) ETOH-600 ($EuTiO_{2.38}N_{0.48}\square_{0.14}$). Both structures were refined using the ideal perovskite structure ($Pm\bar{3}m$). Refined parameters are shown in Table 1. Red crosses, green solid line, and blue solid line represent observed, calculated, and difference intensities, respectively, while green ticks indicate the peak positions.

Surprisingly, a drastic change in the diffraction profiles is recognized when the ammonolysis temperature of $EuTiO_{2.82}H_{0.18}$ is increased. With increasing T_R to 600−800 °C, the obtained XRD peaks are largely shifted to higher angles, meaning a significant contraction of the cell volume. Additionally, we observed, for T_R = 700 and 800 °C, a cubic-to-orthorhombic transition accompanied by the appearance of superstructure reflections, where the enlarged cell is related to the primitive perovskite cell by $\sqrt{2}a_p \times 2b_p \times \sqrt{2}c_p$ (see Figure 3 and Figure S5). These observations suggest a continuous and substantial oxidization of Eu^{2+} to Eu^{3+} with increasing T_R, despite the highly reducing atmosphere of ammonolysis.

Magnetic measurements of ETOH-800 (T_R = 800 °C) revealed that the Eu ion is oxidized completely to +3, strongly suggesting a composition of $Eu^{3+}Ti^{4+}O_2N$. As shown in Figure 1a, nonmagnetic behavior in the temperature dependence of magnetic susceptibility indicates the fully trivalent state in Eu with $4f^6$ (S = 3 and L = 3, thus J = 0). Note that the slight increase in the susceptibility below 15 K (see Figure 1b) is reproduced by a fit based on the Van Vleck theory involving the contribution of the excited states of Eu^{3+}.[18] Details of the Van Vleck theory are described in Supporting Information. The ^{151}Eu Mössbauer spectrum for ETOH-800 at room temperature (Figure 4a) consists only of a single peak with the isomer shift of 0.30(2) mm/s, which is attributed to the resonance absorption of Eu^{3+} nuclei (**3** in Scheme 1).

The occupation of the A-site by Eu^{3+}, which has an ionic radius smaller than that of Eu^{2+} (1.07 Å vs 1.25 Å), leads to a smaller Goldschmidt tolerance factor t.[19] Using tabulated data,[20] we obtained t = 0.89 for $Eu^{3+}TiO_2N$, which is much smaller than t = 0.95 for $Eu^{2+}TiO_3$. Furthermore, the reduced (normalized) volume of 58.690(2) Å^3 in $EuTiO_2N$ (or ETOH-800) relative to $EuTiO_3$ (59.5026 Å^3) as well as the lowered symmetry with the aforementioned superlattice indicates the presence of cooperative TiO_4N_2 octahedral rotations in $EuTiO_2N$.

Given the orthorhombic $\sqrt{2}a_p \times 2b_p \times \sqrt{2}c_p$ cell and small t, it would be quite natural to build a structural model on the basis of the $GdFeO_3$-type structure (space group: $Pnma$),[21]

Table 1. Structural Parameters of ETOH-400 ($EuTiO_{2.82}N_{0.18}$), ETOH-600 ($EuTiO_{2.38}N_{0.48}$), and ETOH-800 ($EuTiO_2N$) from Rietveld Refinement of SXRD Data[a]

atom	Wyckoff site	g[b]	B_{iso} (Å^2)
ETOH-400 ($EuTiO_{2.82}N_{0.12}$)[c]			
Eu	1b, (0.5, 0.5, 0.5)	1	0.508(7)
Ti	1a, (0, 0, 0)	1	0.34(2)
O	3d, (0.5, 0, 0)	0.970(9)	0.73(6)
ETOH-600 ($EuTiO_{2.38}N_{0.48}$)[d]			
Eu	1b, (0.5, 0.5, 0.5)	1	0.73(1)
Ti	1a, (0, 0, 0)	1	0.24(2)
O	3d, (0.5, 0, 0)	0.934(8)	1.82(9)
ETOH-800 ($EuTiO_2N$)[e]			
Eu	8d, (0.0440(1), 0.2496(1), 0.9908(1))	1	0.36(1)
Ti	4b, (0, 0, 0.5)	1	0.47(2)
O1	4c, (0.470(1), 0.25, 0.090(1))	1.00(1)	1.1(1)
O2	8d, (0.2920(9), 0.0442(7), 0.711(1))	1.00(1)[f]	1.1(1)[g]

[a]Values in parentheses for refined parameters indicate one standard deviation. [b]g represents the occupancy of each site. [c]Space group: $Pm\bar{3}m$ (no. 221), a = 3.9103(1) Å, R_{wp} = 10.1%, R_p = 7.7%, χ^2 = 5.9. [d]Space group: $Pm\bar{3}m$ (no. 221), a = 3.9038(1) Å, R_{wp} = 7.5%, R_p = 5.0%, χ^2 = 2.2. [e]Space group: $Pnma$ (no. 62), a = 5.5554(1) Å, b = 7.7470(2) Å, c = 5.4548(1) Å, R_{wp} = 6.6%, R_p = 4.9%, χ^2 = 2.2. [f]Linear constraint: g(O2) = g(O1). [g]Linear constraint: B_{iso}(O2) = B_{iso}(O1).

DOI: 10.1021/jacs.6b00088
J. Am. Chem. Soc. 2016, 138, 3211−3217

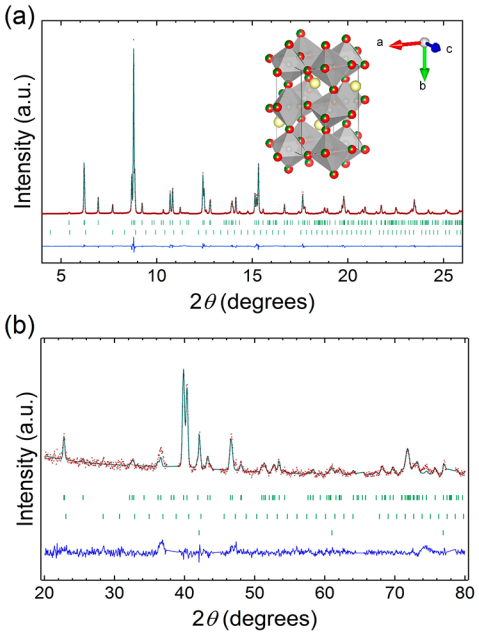

Figure 3. Observed and refined (a) SXRD (λ = 0.420671 Å) and (b) ND (λ = 1.54060 Å) patterns for ETOH-800 ($EuTiO_2N$). Shown in the inset of panel a is the crystal structure of $EuTiO_2N$ with the $GdFeO_3$-type structure (*Pnma*). Red crosses and green and blue solid lines represent observed, calculated, and difference intensities, respectively. The first and the second rows of green ticks indicate the positions of $EuTiO_2N$ and Eu_2O_3 (3.05 wt %) peaks, respectively. The third rows in panel b indicate the peaks of elemental V coming from the cylinder sample holder. Aluminum foil peaks are removed from the data and fitting. Refined parameters for SXRD are shown in Table 1, while those for ND are as follows: R_{wp} = 3.2%, R_p = 2.5%, χ^2 = 1.06, $EuTiO_{2.01(6)}N_{0.99(6)}$, B_{iso}(Eu) = 0.7(1), B_{iso}(Ti) = 0.8(2).

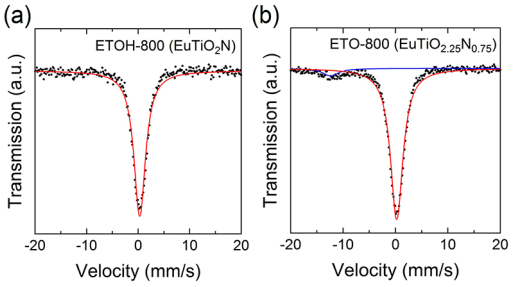

Figure 4. ^{151}Eu Mössbauer spectra of (a) ETOH-800 ($EuTiO_2N$) and (b) ETO-800 ($EuTiO_{2.25}N_{0.75}$) at room temperature. The former spectrum was fitted by a single Lorentzian with an isomer shift of 0.30(4) mm/s and a full width at half-maximum (fwhm) of 2.75(4) mm/s corresponding to Eu^{3+}, while the latter spectrum was fitted by a double Lorentzian with isomer shifts of 0.36(3) mm/s and −12.9(3) mm/s, corresponding to Eu^{3+} and Eu^{2+}, respectively.

with $a^-b^+a^-$ octahedral tilting in Glazer notation.[22] Rietveld refinement of the SXRD data of ETOH-800 (Figure 3a) was conducted with the $GdFeO_3$-type structure placing Eu atoms at the 8d site, Ti atoms at 4b, and O(N) atoms at 4c and 8d. A small amount of impurity Eu_2O_3 (3.05 wt %) was included in the refinement as a secondary phase. The refined parameters are shown in Table 1. When the occupancy of the anion site is allowed to vary, a fully occupied value, $EuTi(O,N)_{3.00(2)}$, is obtained. The orthorhombicity (2.38) of $EuTiO_2N$ was calculated using the obtained lattice parameters.[23] This is remarkably larger than those for known oxynitrides obtained by typical ammonolysis (<1.5), which revealed high distortion of this material.

As shown in Figure 5, the ED patterns of ETOH-800 ($EuTiO_2N$) are fully consistent with the crystallographic data

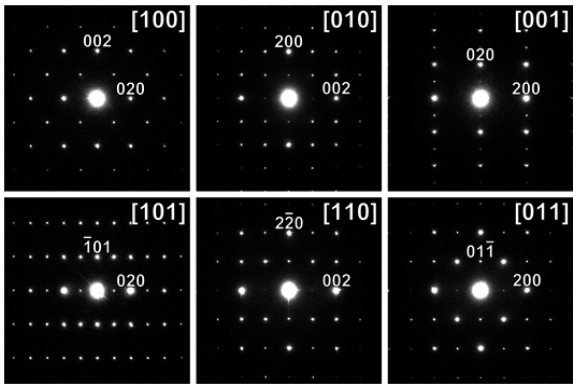

Figure 5. Electron diffraction patterns for ETOH-800 ($EuTiO_2N$), which are indexed consistently with *Pnma* space group. Reflections violating the *h*00: *h* = 2*n*; 0*k*0: *k* = 2*n*; 00*l*: *l* = 2*n* and *hk*0: *h* = 2*n* (in the [010], [001], [101], [110], and [011] ED patterns) reflection conditions imposed by *Pnma* symmetry appear because of multiple diffraction.

(*Pnma*) from SXRD refinement. They also rule out the $P2_1/m$ space group that could be derived from the *cis*-type anion-ordered structure in $SrNbO_2N$ and $SrTaO_2N$ with the d^0 configuration of the B cations.[24,25] Furthermore, the absence of second harmonic generation (SHG) response in $EuTiO_2N$ excludes the acentric subgroups and hence confirms the centric *Pnma* space group. Because the sample contains a small amount of Eu_2O_3 impurity, whose crystals look very similar to those of the target material, each analyzed particle was first tested with energy-dispersive X-ray spectroscopy (EDX) to ensure the presence of Ti.

The large contrast between the neutron scattering lengths of O and N allowed us to determine the anion composition of ETOH-800. The atomic positions were fixed to those determined from the SXRD refinement because of the relatively weak intensity of the ND pattern. A small impurity of Eu_2O_3 was also observed along with elemental V and Al coming, respectively, from the vanadium cylinder sample holder and the aluminum foil. Eu_2O_3 and V were included in the refinement, but Al was excluded due to its strong preferred orientation. Applying the constraint g(O1) + g(N1) = 1, g(O2) + g(N2) = 1, g(O1) = g(O2), and B_{iso}(O1) = B_{iso}(O2) = B_{iso}(N1) = B_{iso}(N2) = 1 on the O/N occupancy factors, the ND profile was refined and we obtained the almost fully stoichiometric composition $EuTiO_{2.01(6)}N_{0.99(6)}$ (see Figure 3b and Table S2). We note that the refinement without the constraint g(O1) = g(O2) did not converge reasonably. Elemental analysis for ETOH-800 gave a nitrogen content of 5.59 wt %, in excellent agreement with the theoretical value of 5.6 wt % for $EuTiO_2N$.

The ammonolysis reaction of the pyrochlore $Eu_2Ti_2O_7$ at 800 °C resulted in decomposition into Eu_2O_3 and unknown phases (Figure S6). This dependence on precursor strongly indicates that $EuTiO_2N$ is a thermodynamically metastable phase only accessible by a topochemical route. It is remarkable that the synthesis of $EuTiO_2N$ requires a rather high temperature (800 °C) in comparison with conventional topochemical reactions to prepare reduced oxides, oxyhalides, and oxyhydrides.[26−29] The

DOI: 10.1021/jacs.6b00088
J. Am. Chem. Soc. 2016, 138, 3211−3217

requirement of such a high temperature for the topochemical ammonolysis is related to the less mobile nature of N^{3-}, due to its higher valence, as theoretically demonstrated for the fluorite-type oxynitride $Fe_{0.25}Ta_{0.75}O_{0.75}N_{0.25}$, where activation barriers for N^{3-} and O^{2-} migration are 5.98 and 1.87 eV, respectively.[10]

Figure 6 illustrates the relationship between the structures of Ln-Ti^{4+}-O-N and the ionic radii of Ln^{3+} (Ln = rare earths). For

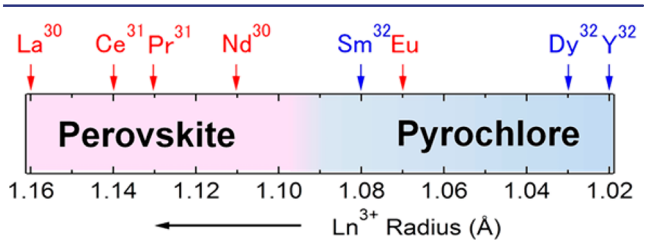

Figure 6. Relationship between the ion radius of the trivalent cation (Ln^{3+}) and the structural types in Ln-Ti^{4+}-O-N systems. Perovskite $LnTiO_2N$ is in red, and pyrochlore $Ln_2Ti_2(O,N)_{7-\delta}$ is in blue. The superscript represents the reference number.

larger Ln^{3+} (La, Ce, Pr, and Nd), perovskite $LnTiO_2N$ is formed,[30,31] while pyrochlore $Ln_2Ti_2(O,N)_{7-\delta}$ is stabilized for smaller Ln^{3+}.[32,33] Gurlo et al.[34] examined existing perovskite oxynitrides, ABO_2N and $ABON_2$, and empirically demonstrated that the stability of the perovskite structure is mainly governed by the tolerance factor t and an octahedral factor d, which is defined by $d = r_B/r_X$, where r_B and r_X denote the ionic radii of the B and X site in ABX_3, respectively (see eq 6 in ref 34). In the case of $LnTiO_2N$ (with $d = 0.422$), the perovskite structure is stable when $0.931 < t < 1.038$, implying that the octahedral tilting is considerably suppressed in oxynitrides, compared with oxides where the perovskite structure exists down to $t \sim 0.75$.[35] The value of t for $EuTiO_2N$ is smaller than the lower limit (0.931), providing a justification that $EuTiO_2N$ is not thermodynamically stable but is metastable at given conditions (in NH_3 atmosphere) and is formed through the topochemical route. In perovskite oxides, covalency is known to stabilize the $GdFeO_3$-type structure with the $a^-b^+a^-$ tilting system compared with other tilting-type structures.[36] Because the N-for-O substitution is expected to enhance the covalency, the observation of the $a^-b^+a^-$ tilting in $EuTiO_2N$ should be reasonable. Such a stable structure of $EuTiO_2N$ as well as the valence variability of Eu ions may be reasons for the introduction of more nitrogen than expected from our studies on $BaTiO_{3-x}H_x$. From these results, high temperature topochemical ammonolysis allows the formation of metastable perovskite oxynitride phases with extensive distortion, which may bring novel magnetic, transport, and optical properties.

To obtain more insight into the reaction mechanism, we performed ammonolysis reactions in a similar fashion but using $EuTiO_3$ and observed distinct results. XRD patterns of ETO-800 are indexed with an orthorhombic $\sqrt{2}a_p \times 2b_p \times \sqrt{2}c_p$ unit cell, as observed in $EuTiO_2N$. However, as shown in Figure 7b, its cell volume is much larger than that of ETOH-800 ($EuTiO_2N$), implying an incomplete nitridation for ETO-800. SXRD refinement assuming the $GdFeO_3$-type structure gave a nearly stoichiometric anion content of 2.97(3) (Figure S7b and Table S3), while elemental analysis gave a nitrogen content of 4.24 wt %, corresponding to $Eu^{2.75+}TiO_{2.25}N_{0.75}$ (**5** in Scheme 1, and Figure 7a). This composition is further supported by a magnetic measurement, yielding a mean valence of $Eu^{2.75+}$ (Figure 1b). The ^{151}Eu Mössbauer spectrum, shown

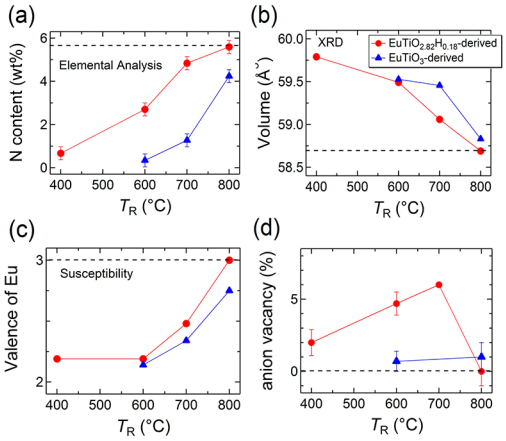

Figure 7. T_R dependence of (a) nitrogen content (from elemental analysis), (b) normalized volume (from Le Bail analysis of XRD), (c) valence state of Eu (from inverse susceptibility) and (d) amount of anion vacancies of $EuTiO_{2.82}H_{0.18}$-derived (red) and $EuTiO_3$-derived oxynitrides (blue). In panel d, amount of anion vacancies is shown by $[y/(x + y)] \times 100$ in $EuTi(O,N)_x\square_y$.

in Figure 4b, is composed of two peaks centered at −12.9(3) mm/s and 0.36(3) mm/s, assigned, respectively, to Eu^{2+} and Eu^{3+}. From the area ratio of the two absorption peaks, the Eu valence was estimated to be 2.94, a little larger than that obtained above. However, this apparent discrepancy can be attributed to the difference in the Debye−Waller factors for Eu^{3+} and Eu^{2+}, as observed in other Eu-containing compounds.[37−39]

All attempts to synthesize the full stoichiometric phase of $EuTiO_2N$ from $EuTiO_3$ by changing the reaction temperature and/or time were unsuccessful. For longer reaction time at 800 °C, the amount of unidentified impurities increased prominently while the nitrogen content only slightly increased. We observed that raising T_R beyond 900 °C resulted in a drastic reduction in the nitrogen content, which is consistent with results of Weidenkaff et al. who synthesized $Eu^{2.04+}Ti^{4+}O_{2.96}N_{0.04}$ by the ammonolysis of $EuTiO_3$ at 950 °C.[40] The significant reduction of Eu here in the perovskite is due to the highly reductive atmosphere at higher T_R. At T_R = 1000 °C, $EuTiO_3$ decomposed into Eu_2O_3 and other unknown phases (Figure S8).

Why was the stoichiometric $EuTiO_2N$ obtained only from $EuTiO_{2.82}H_{0.18}$ and not from $EuTiO_3$? To clarify this, we investigated ammonolyzed samples of $EuTiO_{2.82}H_{0.18}$ and $EuTiO_3$ at intermediate temperatures of 400 °C < T_R < 800 °C (**2** and **4** in Scheme 1). Figures 1a and 7b show that Eu^{2+} in ETOH-600 is only partially oxidized, and the sample composition was determined to be $Eu^{2.2+}TiO_{2.38}N_{0.48}\square_{0.14}$ from elemental analysis, giving the nitrogen content of 2.7 wt %. The Curie−Weiss fitting of the magnetic susceptibility gives a Curie constant C of 6.34(2) emu K mol^{-1} (corresponding to $Eu^{2.2+}$) (Figure 7a, Figure 7c, Figure S9, and Table S4). This composition agrees well with $EuTi(O,N)_{2.80(2)}\square_{0.20}$ derived from the Rietveld analysis of SXRD pattern (Figure 2b and Table 1). Obviously, ETOH-600 has more anion vacancies than ETOH-400 ($EuTiO_{2.82}N_{0.12}\square_{0.06}$). Here, the loss of O^{2-} exceeds the uptake of N^{3-}. More anion vacancies appear at T_R = 700 °C, with an approximate composition of $Eu^{2.46+}TiO_{2.00}N_{0.82}\square_{0.18}$ (Figure 7a, Figure 7d, Figure S9, and Table S4). In contrast, ETO-600 has nearly the same lattice parameter as $EuTiO_3$, and its nitrogen content is only 0.34 wt

DOI: 10.1021/jacs.6b00088
J. Am. Chem. Soc. 2016, 138, 3211−3217

%, which is much smaller than 2.70 wt %, observed for ETOH-600. The absence of a recognizable amount of anion vacancies is found from Rietveld SXRD refinements for ETO-600 and ETO-800 (Figure S7 and Table S3). Thus, the oxidative nitridation of $EuTiO_3$ probably proceeds through a (nearly) 1:1 exchange of N^{3-} with O^{2-}.

Furthermore, let us consider the origin of the remarkable difference in composition of ammonolyzed specimens (at various T_R's) between $EuTiO_3$-derived and $EuTiO_{2.82}H_{0.18}$-derived systems. Because hydride ions in $EuTiO_{2.82}H_{0.18}$ are already lost by the ammonolysis at 400 °C (yielding $EuTiO_{2.82}N_{0.12}\square_{0.06}$), the hydride lability, which has been underlined for $BaTiO_{3-x}H_x$,[41] is clearly not responsible for the drastic N^{3-}/O^{2-} exchange at higher T_R. Instead, the presence of anion vacancies, even with 2 at. % concentration for $EuTiO_{2.82}N_{0.12}\square_{0.06}$, for higher, as more vacancies are created in situ as the sample is heated toward 800 °C, would be therefore of crucial importance for the synthesis of stoichiometric $EuTiO_2N$.

For the $EuTiO_3$-derived system, we do not observe notable concentrations of anion vacancies, but the N^{3-}/O^{2-} exchange or diffusion through the lattice is possible with a help of a finite but very small amount of anion vacancies created during ammonolysis. In such a circumstance with a negligibly small anion vacancy concentration, the energy required for anion (O, N) diffusion would be substantially high, making anion diffusion and exchange possible only above 600 °C (see Figure 7a). In addition, because of the less mobile nature of N^{3-} (vs O^{2-}),[10] the kinetic barriers will be even higher as the N-for-O substitution takes place. These factors could be the reason why the nitridation did not proceed beyond $EuTiO_{2.25}N_{0.75}$ when $EuTiO_3$ was used as a starting compound. On the other hand, the anion exchange (diffusion) in $EuTiO_{2.82}N_{0.12}\square_{0.06}$ with 2 at. % anion deficiency is significantly promoted at low temperature (>400 °C) due to a reduced kinetic barrier for anion diffusion, which allows the facile exchange of N^{3-}/O^{2-} anions, leading finally to the stoichiometric (terminal) phase of $EuTiO_2N$. In oxide ion conductors, it has been well established that the creation of oxygen vacancies is a key parameter to encourage oxygen diffusion, as seen in $Zr_{1-x}Y_xO_{2-0.5x}\square_{0.5x}$ and $La_{0.9}Sr_{0.1}Ga_{0.8}Mg_{0.2}O_{2.85}\square_{0.15}$.[42−44] The present study underlines the importance of the creation of anion vacancies for the topochemical synthesis of oxynitrides and possibly other mixed anion compounds. In other words, by mimicking strategies used in oxide ion conductivity, we are able to achieve precise and versatile control of the anion composition of oxynitrides.

Other than the present result on archetypal perovskite, there are only a few examples of topochemically prepared oxynitrides with a sizable (yet nonstoichiometric) nitrogen content. The pyrochlore oxynitride $Eu_2Mo_2O_{5-x}N_{2+x-\delta}$ ($x < 1$) with a sizable anion vacancy concentration ($\delta/x = 0.15-0.20$) is topochemically synthesized by ammonolysis of $Eu_2Mo_2O_7$ at 600−650 °C.[45] The other two examples are concerned with Dion−Jacobson (DJ) layered perovskite oxides, $LiLaTa_2O_7$ and $RbCa_2Nb_3O_{10}$, topochemically transformed to $LiLaTa_2O_{7-3x}N_{2x}$ ($x = 0.29$) and $Rb_{1+x}Ca_2Nb_3O_{10-x}N_x{\cdot}yH_2O$ ($x = 0.7-0.8$),[46,47] which is understandable given an excellent ion-exchangeability of DJ phases.[48−50] This study demonstrates a unique example of topochemically prepared stoichiometric perovskite oxynitride. We believe that this strategy could be used to convert other titanium perovskite oxides $Ln^{3+}Ti^{3+}O_3$ (Ln = Sm, Gd−Lu and Y) to $LnTi^{4+}O_2N$. This synthetic strategy could be also extended to prepare other transition metal perovskite oxynitrides. While $LnV^{4+}O_2N$ is known to exist only for larger Ln^{3+} cations (La, Pr, and Nd),[51] $LnV^{4+}O_2N$ with smaller Ln^{3+} cations (Sm−Lu and Y) may be yielded through multistep reactions starting from $LnV^{3+}O_3$.

CONCLUSION

We have demonstrated the topochemical synthesis of a heavily nitridized perovskite $EuTiO_3$ via ammonolysis of the pristine oxide and its hydridized form. Interestingly, the stoichiometric and completely oxidized oxynitride phase of $EuTiO_2N$ is only accessible from the oxyhydride ($EuTiO_{2.82}H_{0.18}$), which is attributable to the presence of a small amount of anion vacancy created in situ during the initial nitridation process. In contrast to the conventional topochemical reactions to synthesize highly reduced oxides and other mixed anion compounds,[26−29] the present reaction proceeds at rather high temperatures (~800 °C) that could be related to the difficulty in the nitride anion migration through the oxide lattice. So far, perovskite oxynitrides have been mostly prepared by high temperature ammonolysis using starting reagents such as oxides and carbonates but perhaps without deeper consideration of kinetic aspects that include the diffusion pathway of N^{3-}/O^{2-} anions, the stability of the precursor phase, and the formation of intermediate phases. We thus believe that a number of new oxynitride perovskites (or other structural types) will be discovered through the high temperature topochemical approach, offering a versatile control of composition and structure (octahedral distortion), and hence the properties, of the resulting oxynitrides.

ASSOCIATED CONTENT

Supporting Information

The Supporting Information is available free of charge on the ACS Publications website at DOI: 10.1021/jacs.6b00088.

Fitting of the $\chi-T$ curve for $EuTiO_2N$ by Van Vleck theory, XRD patterns for precursors and ammonolyzed samples, SXRD patterns and refined structural parameters for $EuTiO_{2.82}H_{0.18}$, ETO-600, and ETO-800, TG analysis for $EuTiO_{2.82}H_{0.18}$, and magnetic measurements for precursors and ammonolyzed samples (PDF)

X-ray and neutron crystallographic file (CIF) for compound $EuTiO_2N$ (ZIP)

AUTHOR INFORMATION

Corresponding Author

*kage@scl.kyoto-u.ac.jp

Author Contributions

The manuscript was written through contributions of all authors. All authors have given approval to the final version of the manuscript.

Notes

Certain commercial equipment, instruments, or materials are identified in this document. Such identification does not imply recommendation or endorsement by the National Institute of Standards and Technology nor does it imply that the products identified are necessarily the best available for the purpose.

The authors declare no competing financial interest.

ACKNOWLEDGMENTS

This work was supported by CREST project and JSPS Grant-in-Aid for Scientific Research (A) (no. 25249090 and no.

DOI: 10.1021/jacs.6b00088
J. Am. Chem. Soc. 2016, 138, 3211−3217

24248016) and for Scientific Research on Innovative Areas "Nano Informatics" (no. 26106514). The synchrotron radiation experiments were performed at the BL02B2 of SPring-8 with the approval of the Japan Synchrotron Radiation Research Institute (JASRI) (proposal nos. 2015B1110, 2015B1111, and 2015B1472). The authors thank Tsukasa Matsubara for his support during an SHG measurement.

REFERENCES

(1) Kasahara, A.; Nukumizu, K.; Hitoki, G.; Takata, T.; Kondo, J. N.; Hara, M.; Kobayashi, H.; Domen, K. *J. Phys. Chem. A* **2002**, *106*, 6750.
(2) Kasahara, A.; Nukumizu, K.; Takata, T.; Kondo, J. N.; Hara, M.; Kobayashi, H.; Domen, K. *J. Phys. Chem. B* **2003**, *107*, 791.
(3) Kim, Y-II.; Woodward, P. M.; Baba-Kishi, K. Z.; Tai, C. W. *Chem. Mater.* **2004**, *16*, 1267.
(4) Oka, D.; Hirose, Y.; Kamisaka, H.; Fukumura, T.; Sasa, K.; Ishii, S.; Matsuzaki, H.; Sato, Y.; Ikuhara, Y.; Hasegawa, T. *Sci. Rep.* **2014**, *4*, 4987.
(5) Jorge, A. B.; Oró-Solé, J.; Bea, A. M.; Mufti, N.; Palstra, T. T. M.; Rodgers, J. A.; Attfield, J. P.; Fuertes, A. *J. Am. Chem. Soc.* **2008**, *130*, 12572.
(6) Yang, M.; Oró-Solé, J.; Kusmartseva, A.; Fuertes, A.; Attfield, J. P. *J. Am. Chem. Soc.* **2010**, *132*, 4822.
(7) Fuertes, A. *J. Mater. Chem.* **2012**, *22*, 3293.
(8) Sun, S. K.; Motohashi, T.; Masubuchi, Y.; Kikkawa, S. *J. Eur. Ceram. Soc.* **2014**, *34*, 4451.
(9) Smyth, D. M. *Annu. Rev. Mater. Sci.* **1985**, *15*, 329.
(10) Wolff, H.; Dronskowski, R. *Solid State Ionics* **2008**, *179*, 816.
(11) Yajima, T.; Takeiri, F.; Aidzu, K.; Akamatsu, H.; Fujita, K.; Yoshimune, W.; Ohkura, M.; Lei, S.; Gopalan, V.; Tanaka, K.; Brown, C. M.; Green, M. A.; Yamamoto, T.; Kobayashi, Y.; Kageyama, H. *Nat. Chem.* **2015**, *7*, 1017.
(12) Masuda, N.; Kobayashi, Y.; Hernandez, O.; Bataille, T.; Paofai, S.; Suzuki, H.; Ritter, C.; Ichijo, N.; Noda, Y.; Takegoshi, K.; Tassel, C.; Yamamoto, T.; Kageyama, H. *J. Am. Chem. Soc.* **2015**, *137*, 15315.
(13) Yamamoto, T.; Yoshii, R.; Bouilly, G.; Kobayashi, Y.; Fujita, K.; Kususe, Y.; Matsushita, Y.; Tanaka, K.; Kageyama, H. *Inorg. Chem.* **2015**, *54*, 1501.
(14) Izumi, F.; Momma, K. *Solid State Phenom.* **2007**, *130*, 15.
(15) Brous, J.; Fankuchen, I.; Banks, E. *Acta Crystallogr.* **1953**, *6*, 67.
(16) Chien, C. L.; Sleight, A. W. *Phys. Rev. B: Condens. Matter Mater. Phys.* **1978**, *18*, 2031.
(17) McGuire, T. R.; Shafer, M. W.; Joenk, R. J.; Alperin, H. A.; Pickart, S. J. *J. Appl. Phys.* **1966**, *37*, 981.
(18) Takikawa, Y.; Ebisu, S.; Nagata, S. *J. Phys. Chem. Solids* **2010**, *71*, 1592.
(19) Goldschmidt, V. M. *Skrifter Norsk. Vid. Akademie, Oslo, Mat. Nat. Kl.* **1926**, *KI8*.
(20) Shannon, R. D. *Acta Crystallogr., Sect. A: Cryst. Phys., Diffr., Theor. Gen. Crystallogr.* **1976**, *32*, 751.
(21) Geller, S. *J. Chem. Phys.* **1956**, *24*, 1236.
(22) Woodward, P. M. *Acta Crystallogr., Sect. B: Struct. Sci.* **1997**, *53*, 32.
(23) Vasylechko, L.; Akselrud, L.; Matkovskii, A.; Sugak, D.; Durygin, A.; Frukacz, Z.; Lukasiewicz, T. *J. Alloys Compd.* **1996**, *242*, 18.
(24) Yang, M.; Oró-Solé, J.; Rodgers, J. A.; Jorge, A. B.; Fuertes, A.; Attfield, J. P. *Nat. Chem.* **2011**, *3*, 47.
(25) Attfield, J. P. *Cryst. Growth Des.* **2013**, *13*, 4623.
(26) Hayward, M. A.; Cussen, E. J.; Claridge, J. B.; Bieringer, M.; Rosseinsky, M. J.; Kiely, C. J.; Blundell, S. J.; Marshall, I. M.; Pratt, F. L. *Science* **2002**, *295*, 1882.
(27) Tsujimoto, Y.; Tassel, C.; Hayashi, N.; Watanabe, T.; Kageyama, H.; Yoshimura, K.; Takano, M.; Ceretti, M.; Ritter, C.; Paulus, W. *Nature* **2007**, *450*, 1062.
(28) Murphy, D. W.; Greenblatt, M.; Cava, R. J.; Zahurak, S. M. *Solid State Ionics* **1981**, *5*, 327.
(29) Kobayashi, Y.; Tian, M.; Eguchi, M.; Mallouk, T. E. *J. Am. Chem. Soc.* **2009**, *131*, 9849.
(30) Clarke, S. J.; Guinot, B. P.; Michie, C. W.; Calmont, M. J. C.; Rosseinsky, M. J. *Chem. Mater.* **2002**, *14*, 288.
(31) Porter, S. H.; Huang, Z.; Cheng, Z.; Avdeev, M.; Chen, Z.; Dou, S.; Woodward, P. M. *J. Solid State Chem.* **2015**, *226*, 279.
(32) Dolgikh, V. A.; Lavut, E. A. *Russ. J. Inorg. Chem.* **1991**, *36*, 1389.
(33) Subramanian, M. A.; Aravamudan, G.; Subba Rao, G. V. *Prog. Solid State Chem.* **1983**, *15*, 55.
(34) Li, W.; Ionescu, E.; Riedel, R.; Gurlo, A. *J. Mater. Chem. A* **2013**, *1*, 12239.
(35) Weis, R. S.; Gaylord, T. K. *Appl. Phys. A: Solids Surf.* **1985**, *37*, 191.
(36) Woodward, P. M. *Acta Crystallogr., Sect. B: Struct. Sci.* **1997**, *53*, 44.
(37) Zong, Y.; Fujita, K.; Akamatsu, H.; Murai, S.; Tanaka, K. *J. Solid State Chem.* **2010**, *183*, 168.
(38) Furuuchi, F.; Wakeshima, M.; Hinatsu, Y. *J. Solid State Chem.* **2004**, *177*, 3853.
(39) Zhai, H. F.; Zhang, P.; Wu, S. Q.; He, C. Y.; Tang, Z. T.; Jiang, H.; Sun, Y. L.; Bao, J. K.; Nowik, I.; Felner, I.; Zeng, Y. W.; Li, Y. K.; Xu, X. F.; Tao, Q.; Xu, Z. A.; Cao, G. H. *J. Am. Chem. Soc.* **2014**, *136*, 15386.
(40) Sagarna, L.; Rushchanskii, K. Z.; Maegli, A.; Yoon, S.; Populoh, S.; Shkabko, A.; Pokrant, S.; Ležaić, M.; Waser, R.; Weidenkaff, A. *J. Appl. Phys.* **2013**, *114*, 033701.
(41) Kobayashi, Y.; Hernandez, O. J.; Sakaguchi, T.; Yajima, T.; Roisnel, T.; Tsujimoto, Y.; Morita, M.; Noda, Y.; Mogami, Y.; Kitada, A.; Ohkura, M.; Hosokawa, S.; Li, Z.; Hayashi, K.; Kusano, Y.; Kim, J. E.; Tsuji, N.; Fujiwara, A.; Matsushita, Y.; Yoshimura, K.; Takegoshi, K.; Inoue, M.; Takano, M.; Kageyama, H. *Nat. Mater.* **2012**, *11*, 507.
(42) Goodenough, J. B. *Annu. Rev. Mater. Res.* **2003**, *33*, 91.
(43) Goff, J. P.; Hayes, W.; Hull, S.; Hutchings, M. T.; Clausen, K. N. *Phys. Rev. B: Condens. Matter Mater. Phys.* **1999**, *59*, 14202.
(44) Ishihara, T.; Matsuda, H.; Takita, Y. *J. Am. Chem. Soc.* **1994**, *116*, 3801.
(45) Yang, M.; Oró-Solé, J.; Fuertes, A.; Attfield, J. P. *Chem. Mater.* **2010**, *22*, 4132.
(46) Lee, E.; Kim, S. J; Paik, Y.; Kim, Y-II. *Mater. Res. Bull.* **2013**, *48*, 813.
(47) Schottenfeld, J. A.; Benesi, A. J.; Stephens, P. W.; Chen, G.; Eklund, P. C.; Mallouk, T. E. *J. Solid State Chem.* **2005**, *178*, 2313.
(48) Schaak, R. E.; Mallouk, T. E. *Chem. Mater.* **2002**, *14*, 1455.
(49) Kodenkandath, T. A.; Lalena, J. N.; Zhou, W. L.; Carpenter, E. E.; Sangregorio, C.; Falster, A. U.; Simmons, W. B., Jr.; O'Connor, C. J.; Wiley, J. B. *J. Am. Chem. Soc.* **1999**, *121*, 10743.
(50) McIntyre, R. A.; Falster, A. U.; Li, S.; Simmons, W. B., Jr.; O'Connor, C. J.; Wiley, J. B. *J. Am. Chem. Soc.* **1998**, *120*, 217.
(51) Oró-Solé, J.; Clark, L.; Kumar, N.; Bonin, W.; Sundaresan, A.; Attfield, J. P.; Rao, C. N. R.; Fuertes, A. *J. Mater. Chem. C* **2014**, *2*, 2212.

DOI: 10.1021/jacs.6b00088
J. Am. Chem. Soc. 2016, 138, 3211−3217